Interplay of Surface Diffusion and Surface Tension in the Evolution of Solid/Liquid Interfaces. Dealloying of β-Brass in Aqueous Sodium Chloride

H. Martín,[†] P. Carro,[†] A. Hernández Creus,[†] J. Morales,[†] G. Fernández,[†] P. Esparza,[‡] S. González,[†] R. C. Salvarezza,[§] and A. J. Arvia*[,§]

Departamento de Química Fisica, Facultad de Química, and Departamento de Química Inorgánica, Facultad de Química, Universidad de La Laguna, Spain, and Instituto de Investigaciones Fisicoquimicas Teóricas y Aplicadas (INIFTA) (UNLP-CONICET-CIC Bs.As.), Sucursal 4, Casilla de Correo 16, (1900) La Plata, Argentina

Received: March 22, 2000

The dealloying of β-brass in 0.5 M aqueous NaCl was studied by electrochemical techniques at different temperatures in the range 278 K ≤ T ≤ 318 K, complemented with in situ scanning tunneling microscopy (STM) imaging. In the potential region where the electrodissolution of zinc and the formation of vacancies and copper islands take place, two different roughness regimes were distinguished. When dealloying involves only a few monolayers (ML) the process approaches a quasiuniform alloy electrodissolution, whereas after electrodissolution of more than 20 ML, void formation takes place. In both regimes the interface evolution was analyzed by applying the dynamic scaling method to in situ STM imaging data. The first roughness regime exhibits a stable interface consisting of copper-rich islands that coarsen with time according to a surface diffusion controlled process. The second roughness regime exhibits an unstable interface due to a curvature dependent corrosion rate enhancing zinc electrodissolution at cavities. The overall interface evolution is well-described by a differential stochastic equation containing an electrodissolution term and surface rearrangement terms related to surface diffusion and negative surface tension effect.

1. Introduction

Multicomponent solid materials such as metal alloys in contact with a liquid or a gas phase may undergo, under certain conditions, an environmentally induced loss of one component. In this case, the properties of the material, in general, and its surface properties, in particular, can be drastically modified. Therefore, this issue stands as a serious challenge in material sciences. Among selective dissolution processes, dealloying is an important, although far less understood process, in metallic corrosion.[1−3] It occurs either spontaneously or within a certain applied potential window usually close to the open circuit potential of the alloy in the aggressive environment.

For a binary alloy, dealloying involves the electrodissolution of the most reactive component (MRC), the less reactive component (LRC) remaining immune. Accordingly, on the surface of the dissolving alloy a layer rich in LRC, which slows down further electrodissolution of the alloy, is formed.[2] In some cases, dealloying leads to the redistribution of the LRC remnants, and nanopore formation that may result in pitting corrosion.[4]

Binary alloys such as brass (copper−zinc alloys), a type of material widely used for technical applications, can be considered as model systems to study the kinetics and mechanism of dealloying in aqueous aggressive environments by applying electrochemical methods.[5,6] In fact, the electrodissolution of brass in such environments at the rate of a few microamperes per centimeter squared yields soluble Zn^{2+} ionic species and copper islands distributed over the specimen surface.

Two main models have been proposed to describe binary alloy dealloying kinetics, depending on whether the diffusion of vacancies in the bulk of the alloy[7,8] or the LRC surface diffusion[9] is considered as rate-controlling step. In principle, the dealloying mechanism should be reflected in the evolution of the topography during electrodissolution. Then, the study of the dynamics of the alloy/aggressive environment interface[10] becomes of increasing interest to investigate the formation and destruction mechanism of solid phases, a crucial issue for controlling the performance of materials and improving solid surface morphology and quality.

Interface evolution data can be interpreted using the dynamic scaling theory.[10,11] For a solid of size L, this theory predicts that the interface width, ξ, increases with t, the duration of the process, as $\xi \propto t^{\beta}$ for $t \to 0$, and with L as $\xi \propto L^{\alpha}$ for $t \to \infty$. The interface width corresponds to the mean root square roughness of the growing surface. The values of α, β, and z (=α/β), i.e., the static, growth, and dynamic exponents, respectively, depend on the physical process dominating the interface dynamics. In a previous paper,[12] the role of surface diffusion in the evolution of the interface was inferred from the dynamic scaling of ex situ STM images of β-brass surfaces undergoing dealloying in aqueous 0.5 M sodium chloride. In this case, the value α = 0.8 was consistent with a surface diffusion controlled dealloying process,[11] although values of β and z that are required for a complete characterization of the interface could not be determined.

This work provides a complete characterization of the interface dynamics for β-brass dealloying in aqueous 0.5 M sodium chloride from in situ scanning tunneling microscopy (STM), electrochemical, scanning electron microscopy (SEM), and energy dispersion X-ray analysis (EDAX) data. Experimental results are consistent with a complex process in which dealloying leads to the formation of soluble Zn^{2+} complex ions,

[†] Departamento de Química Fisica, Universidad de La Laguna.
[‡] Departamento de Química Inorgánica, Universidad de La Laguna.
[§] Instituto de Investigaciones Fisicoquimicas Teóricas y Aplicadas.

10.1021/jp001077c CCC: $19.00
Published on Web 08/04/2000

vacancies at the alloy surface, and copper adatoms. The kinetics of the overall reaction is determined by the surface diffusion of copper atoms via copper atom−chloride ion interactions. After removing several layers of zinc the interface dynamics exhibits a transition from a stable to an unstable roughness regime. This transition results from the interplay between the surface diffusion of copper atoms and a negative surface tension effect resulting from copper phase formation (islands) and void formation by vacancy aggregation. The negative surface tension term results from the enhancement of zinc electrodissolution at voids. The overall interface evolution can be described by a differential stochastic equation containing an electrodissolution term and surface rearrangement terms related to surface diffusion and negative surface tension effect.

2. Experimental Section

Electrochemical measurements were performed in aqueous 0.5 M sodium chloride in the temperature range 278 K $\leq T \leq$ 318 K using a conventional glass-made electrochemical cell placed in a water thermostat (±0.1 °C). A three-electrode arrangement consisting of a β-brass (47% Zn, 53% Cu) working electrode (0.5 cm^2 apparent surface area), a large area platinum counter electrode facing the working electrode, and a saturated calomel reference electrode (SCE) were utilized.

Working electrodes were prepared by casting and melting as described in ref 12. Each working electrode was wet-polished using different grain size emery papers and finished with 1 μm grit alumina paste. Then, they were successively rinsed with distilled acetone in an ultrasonic bath and twice distilled water and, finally, dried in air at room temperature. To relieve internal stress without affecting the properties of specimens, a heat-treating process was carried out at 150 °C for 2 h under low argon pressure.[13] This treatment, which also improved the surface homogeneity of specimens, assured the reproducibility of the results. After etching treated specimens in acid $FeCl_3$, a grain size density close to 50 grain/cm^2 was found, i.e., the alloy was formed by large grains so that a 1 × 1 μm^2 STM imaging was adequante to characterize a single grain surface. STM images (1 × 1 μm^2) on the noncorroded specimen showed a relatively smooth topography with a root-mean-square roughness (ξ) value close to 1.9 nm.

Single triangular potential sweeps were run at 0.05 V/s from −1.5 to −0.25 V. Polarization curves were recorded at 0.005 V/s from $E = -0.68$ up to −0.2 V with quiescent and stirred solutions. Potentiostatic current transients were recorded by stepping the potential from $E = -0.8$ to −0.45 V. Open circuit potential measurements were also made. Solutions were prepared from sodium chloride (analytical reagent) and triply distilled water. Working solutions were saturated with purified argon for a 2 h gas bubbling before each run.

In situ STM imaging was done at 298 K using a Nanoscope IIE instrument (Santa Barbara, CA) in a KEL-F-made electrochemical cell. In this case, a β-brass working electrode of 1 cm^2 apparent surface area, a platinum counter electrode, and a Pd/H_2 reference electrode were used. To decrease the contributions of faradaic currents, Apiezon-covered Pt−Ir nanotips were used. The following are typical tunneling conditions: tip potential $E_{tip} = 0.35$ V, tunneling current $i_t = 10$ nA, and tunneling voltage $E_t = 0.25$ V. The in situ STM imaging of a smooth surface domain of a large β-brass crystal under null net current was made first. Under this condition, no appreciable changes in the β-brass topography and surface roughness due to drift effects were observed, at least after in situ imaging of the same domain for 10 min. Dealloying of β-brass was investigated under galvanostatic conditions (apparent current density $j = 10$ μA/cm^2) for the time interval $0 \leq t \leq 100$ s.

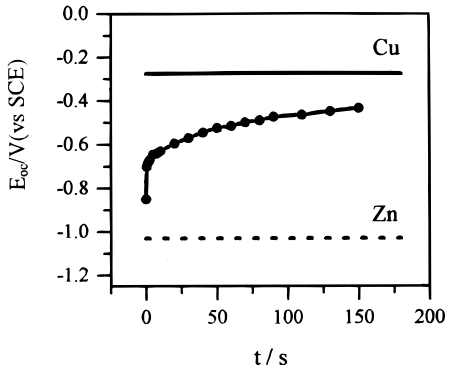

Figure 1. Open circuit potential (E_{oc}) vs time plot for β-brass in aqueous 0.5 M sodium chloride (black dots). The steady open circuit potential at 298 K for copper (full trace) and zinc (dashed trace) are indicated.

Additional scanning electron microscopy (SEM) and energy-dispersive X-ray analysis (EDAX) data for β-brass specimens after dealloying for 1 h at $j = 10$ μA/cm^2 were obtained using conventional instruments.

The potentials (E) in the text are always referred to the SCE scale.

3. Results

3.1. Electrochemical Data. *3.1.1. Open Circuit Potential.* The open circuit potential (E_{oc}) for β-brass specimens in aqueous 0.5 M sodium chloride was followed for 5 h at 298 K. The specimens were first held for 120 s at $E = -0.85$ V to electroreduce possible air-formed surface oxide species, and then the current was switched off to follow the evolution of E_{oc} (Figure 1). Initially, E_{oc} increases from −0.7 to −0.40 V in approximately 50 s to reach $E_{oc} \cong -0.32$ V after $t = 5$ h. It should be noted that for all specimens under comparable experimental conditions (Figure 1), values in the range -0.40 V $< E_{oc} < -0.32$ V are only slightly more negative than the value of E_{oc} for copper and ca. 0.6 V more positive than that of zinc.

The change in E_{oc} is a first indication of the spontaneous dealloying of β-brass in 0.5 M sodium chloride under open circuit conditions and dynamic characteristics of the specimen surface. This makes STM imaging of the topography of the initial β-brass surface practically impossible, as typical imaging for 1 × 1 μm^2 requires about 1 min, a longer time than that involved in surface changes.

3.1.2. Voltammetry Data. Voltammograms of β-brass run in aqueous 0.5 M sodium chloride at 5×10^{-2} V/s and different temperatures (Figure 2) show two broad conjugated pairs of current peaks (AI/CI and AI′/CI′) in the potential range -1.2 V $< E < -0.6$ V. These peaks have been related to the electrodissolution/electrodeposition of zinc.[12] On the other hand, the small pair of peaks AII/CII at −0.45 V has been assigned to the chloride ion electroadsorption/electrodesorption at the copper-rich surface resulting from zinc electrodissolution.[12] The adsorption of chloride ions on copper leads to the formation of a CuCl layer.[14] As temperature is decreased from 318 to 278 K, the charge involved in the current peaks decreases, although the voltammetric features remain qualitatively the same.

Polarization curves recorded at 5×10^{-3} V/s from $E = -0.9$ V upward at different T (Figure 3) show first a broad anodic current peak followed by a nearly constant current density (j_L)

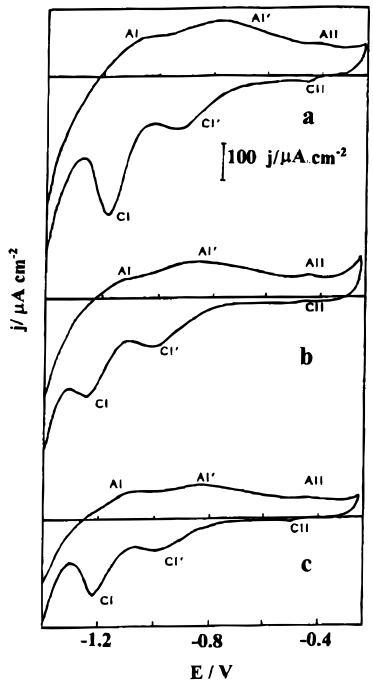

Figure 2. Voltammograms for β-brass in aqueous 0.5 M sodium chloride run at 0.05 V/s at 318 K (a), 298 K (b), and 278 K (c).

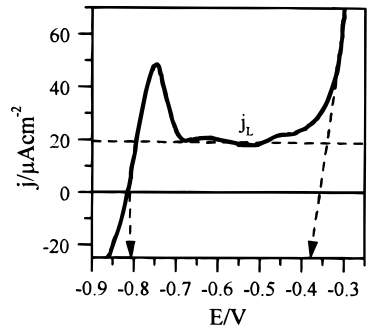

Figure 3. Anodic polarization curve for β-brass in aqueous 0.5 M sodium chloride run at $\upsilon = 0.005$ V/s at 298 K. The horizontal dashed trace indicates the dealloying limiting current (j_L). $E_{oc} = -0.81$ V for $t = 0$. $E_c = -0.38$ V is the upper potential limit for the selective electrodissolution of zinc.

in which two broad anodic peaks of small height are superimposed. These peaks are remnants of peaks AI and AII shown in Figure 2. This apparent current plateau extends over a potential range that decreases as the temperature is increased. As the upper potential limit for the selective electrodissolution of zinc (E_c) is reached, a remarkable increase in j can be observed, the value of E_c decreasing with temperature. After anodizing at $E < E_c$, atomic absorption spectroscopy data only show the appearance of soluble Zn^{2+} species. Conversely, for $E > E_c$ both soluble Cu^{2+}[14] and Zn^{2+} ions can be detected.[12]

Voltammetric data are independent of the rotation speed of the working electrode in the range 0−2000 rpm. Thus, the contribution of mass transport from the solution side to the overall electrochemical process does not have to be considered.

3.1.3. Potentiostatic Current Transients. Potentiostatic current transients (j vs t plots) were recorded at $E = -0.45$ V, a value lying in the potential range of the anodic current plateau in the polarization curves (Figure 3). These current transients fit a $j \propto t^{-0.75}$ relationship for 0 s $\leq t \leq$ 100 s (Figure 4a), in agreement with previously reported data for β-brass dealloying.[6,12] For $t >$ 200 s, a stationary anodic current density is attained. The

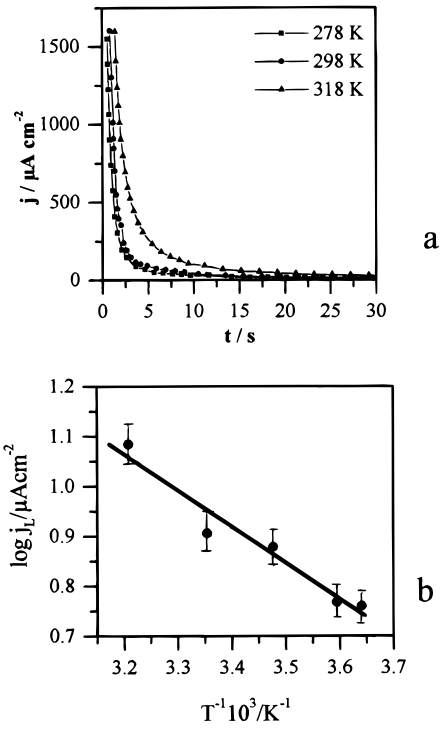

Figure 4. (a) Anodic current density transients run at $E = -0.45$ V and different temperatures. Aqueous 0.5 M sodium chloride. Symbols correspond to experimental data and full traces represent eq 1. (b) Arrhenius plot for steady anodic limiting current densities resulting from current transients.

time dependence of the dealloying current is given by

$$j = j_L + t^{-0.75} \quad (1)$$

as it can be seen in Figure 4.

The charge derived from potentiostatic current transients and the anodic limiting current (j_L) increase with temperature in the range 278−318 K. Values of j_L derived from current transients for $t >$ 200 s were plotted as log j_L vs $1/T$ (Figure 4b). These data can be adjusted by a straight line, and from the slope of this line an apparent activation energy $\Delta E_a^* = 12 \pm 4$ kJ/mol was obtained. In principle, this figure may be related to the activation energy of a diffusion-controlled process from the solution side.[15] This possibility, however, can be discarded because no dependence of j_L on the solution stirring was observed.

The validity of eq 1 is consistent with β-brass dealloying kinetics under surface diffusion control.[6,12] Accordingly, the value of ΔE_a^* can be related to the activation energy of copper atom surface diffusion on either a copper-rich alloy surface or a copper surface.

3.2. SEM Micrographs and EDAX Analysis Data. SEM micrographs (Figure 5) of β-brass surfaces after anodization at −0.48 V ($E < E_c$) for 1 h show a few micron-sized islands and a high surface density of 100−300 nm-sized islands, most ot them appearing at the background in the micrograph. The largest islands appear as bright spots in the micrograph. Voids produced by dealloying can be also observed, most of them 100−300 nm in size. EDAX of the largest islands shows that they are copper-rich.

3.3. Results from in situ STM Imaging. *3.3.1. Sequential STM Imaging*. Sequential in situ STM images (1500 × 1500 nm^2) of the initial β-brass surface taken after immersion at a net null current ($E_{oc} \approx -0.8$ V) show a low roughness

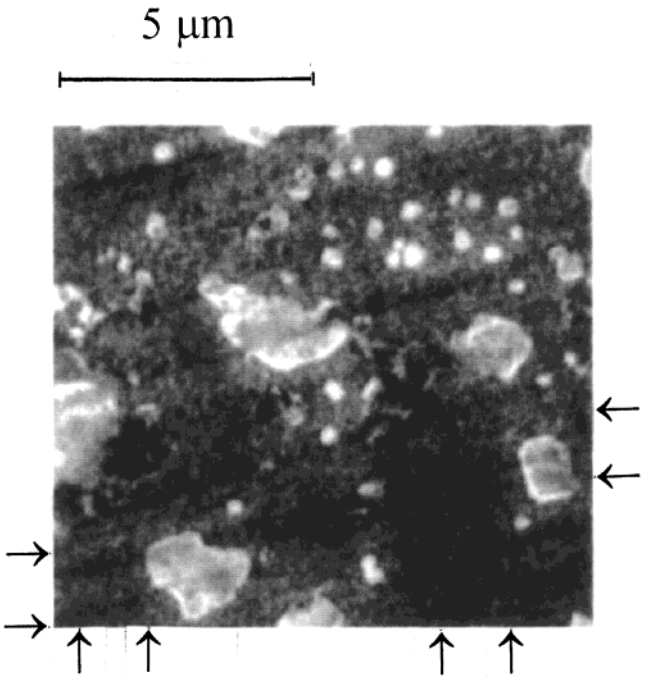

Figure 5. SEM micrograph of β-brass after 1 h anodization in aqueous 0.5 M sodium chloride at $E = -0.48$ V. The arrow indicates typical 1.5×1.5 μm^2-sized domains to be scanned by STM.

topography of terraces and steps (Figure 6a). Each STM image capture takes about 40 s; in this time interval E_{oc} changes from -0.8 to -0.5 V (Figure 1). Accordingly, the STM image taken as reference ($t = 0$) actually corresponds to the image of a β-brass surface mostly covered by copper. However, in this period of time no change in the topography of the specimen at the nanometer to micrometer intermediate range could be observed, suggesting that only zinc from the first layer has been removed.

The STM image (Figure 6b) resulting after 3 min at $j = 10$ μA/cm^2 (Figure 6b) shows the formation of rounded islands following the direction of steps in Figure 6a. These islands of $\langle d \rangle = 160$ nm in average diameter (Figure 7, profile B) correspond to those copper-rich islands that are observed by SEM (Figure 5). The surface of each island is very smooth, as concluded from the cross section analysis of STM images (Figure 7, profile B). The value of $\langle d \rangle$ increases slowly with time but, after removing about 20 zinc atom layers ($t = 30$ min) (Figure 6c), voids are detected (Figure 6d−f). For $t > 30$ min (Figure 6d), the limiting value $\langle d \rangle = 370$ nm is reached, while voids continue growing in depth into bulk alloy. It should be noted that under galvanostatic dealloying ($j_L = 10$ μA/cm^2), the value of E remains close to E_{oc} ($E = -0.360 \pm 0.003$ V).

3.3.2. Kinetics of Copper Island Growth. STM images (Figure 6) and their cross section analysis (Figure 7) show that copper islands increase in size, obeying a linear $\langle d \rangle^4 \propto t$ relationship in the range $0 \leq t \leq 30$ min until the average island diameter is $\langle d \rangle \cong 250$ nm (Figure 8a). Correspondingly, in the range of time in which the relationship $\langle d \rangle^4 \propto t$ is obeyed, the number of islands (N) decreases as $N \propto t^{-1/2}$ (Figure 8b). The dependence of $\langle d \rangle$ and N on time are characteristic of a growth process controlled by surface diffusion.[11] In the range 30 min $\leq t \leq$ 50 min a rapid increase in the average size of islands results in the constant value $\langle d \rangle \cong 300$ nm for $t > 30$ min. Then, the preferred increase in the height of protrusions is observed.

3.3.3. Dynamic Scaling Analysis. The dynamic scaling analysis of STM images is displayed as log ξ vs log t (Figure 9a) and log ξ vs log L (Figure 9b) plots. In the range $0 \leq t \leq$ 30 min, the log ξ vs log t plot yields a straight line with the slope $\beta = 0.21 \pm 0.05$, as expected for an interface evolution dominated by surface diffusion that results in a stable roughness regime.[11] Conversely, for $t > t_c = 30$ min, the log ξ vs log t plot leads to a straight line with the slope $\beta = 0.90 \pm 0.05$, a figure that is consistent with the development of voids that penetrate into the alloy, producing a remarkable increase in roughness. This value of β indicates that the dissolving interface is under an unstable roughness regime after the electrodissolution of several zinc atom layers. Therefore, the value $t_c = 30$ min can be considered as a dealloying transition time that is related to the change from a stable to an unstable roughness regime.

For $t = t_c$ and $L < \langle d \rangle$, the log ξ vs log L plot leads to a straight line with a slope $\alpha = 0.82 \pm 0.05$ (Figure 9b), whereas for $L > \langle d \rangle$ the value of ξ becomes practically constant. The crossover length L_c is related to the limiting value of $\langle d \rangle \cong 300$ nm. It represents the predominant wavelength of copper islands formed during β-brass dealloying and determines the boundary between the stable and the unstable interface evolution regime.

4. Discussion

4.1. Spontaneous Dealloying of β-Brass in Aqueous 0.5 M Sodium Chloride. The open circuit potential of β-brass in the oxygen-free sodium chloride aqueous solution for $t = 0$ (Figure 1) is very close to the potential of null current resulting from the polarization curves (Figure 3). These curves show a rapid increase in current, either cathodic or anodic, as the potential is shifted negatively or positively with respect to the potential of null current. Therefore, the value of E_{oc} actually corresponds to the corrosion potential of β-brass in this environment.

From thermodynamic predictions,[16] the spontaneous dealloying of β-brass in an oxygen-free aqueous solution involves the electrodissolution of zinc and the evolution of hydrogen. In fact, the equilibrium potentials ($E_{r,i}$ where i = Zn or H) of these reactions at 298 K are[16]

$$E_{r,Zn}\,(\text{vs SCE})/\text{V} = -1.010 - 0.0295[\log a(Zn^{2+}) - \log a(Zn^0)] \quad (2)$$

and

$$E_{r,H}\,(\text{vs SCE})/\text{V} = -0.243 - 0.0591[\text{pH} - {}^1/_2 \log P_{H_2}] \quad (3)$$

where the a(i) values denote the activity of the ith constituent in either the solution or the alloy, and P_{H_2} refers to the hydrogen gas pressure. Accordingly, for $t = 0$, $a(Zn^0) \cong 0.5$, $a(Zn^{2+}) = 0$, pH = 7, and $P_{H_2} = 0$, result in $E_{r,Zn} \rightarrow -\infty$ and $E_{r,H} \rightarrow \infty$. Then, the spontaneous reaction can be written as

$$2H^+(aq) + \beta\text{-brass(Cu,Zn)} = H_2 + Zn^{2+}(aq) + \beta\text{-brass(Cu)} \quad (4)$$

where (Cu) indicates that a copper-rich layer is built up on the β-brass surface. The driven force for the spontaneous electrodissolution of zinc should be given by the potential difference between the anodic and cathodic areas at the β-brass surface that are involved in global reaction 4.

From the standpoint of electrochemical kinetics, the slow discharge of either hydrogen ions or water on zinc can be considered as the rate-determining step of reaction 4,[17]

$$H_3O^+ + Zn + e^- \rightarrow Zn(H) + H_2O \quad (5a)$$

$$H_2O + Zn + e^- \rightarrow Zn(H) + OH^- \quad (5b)$$

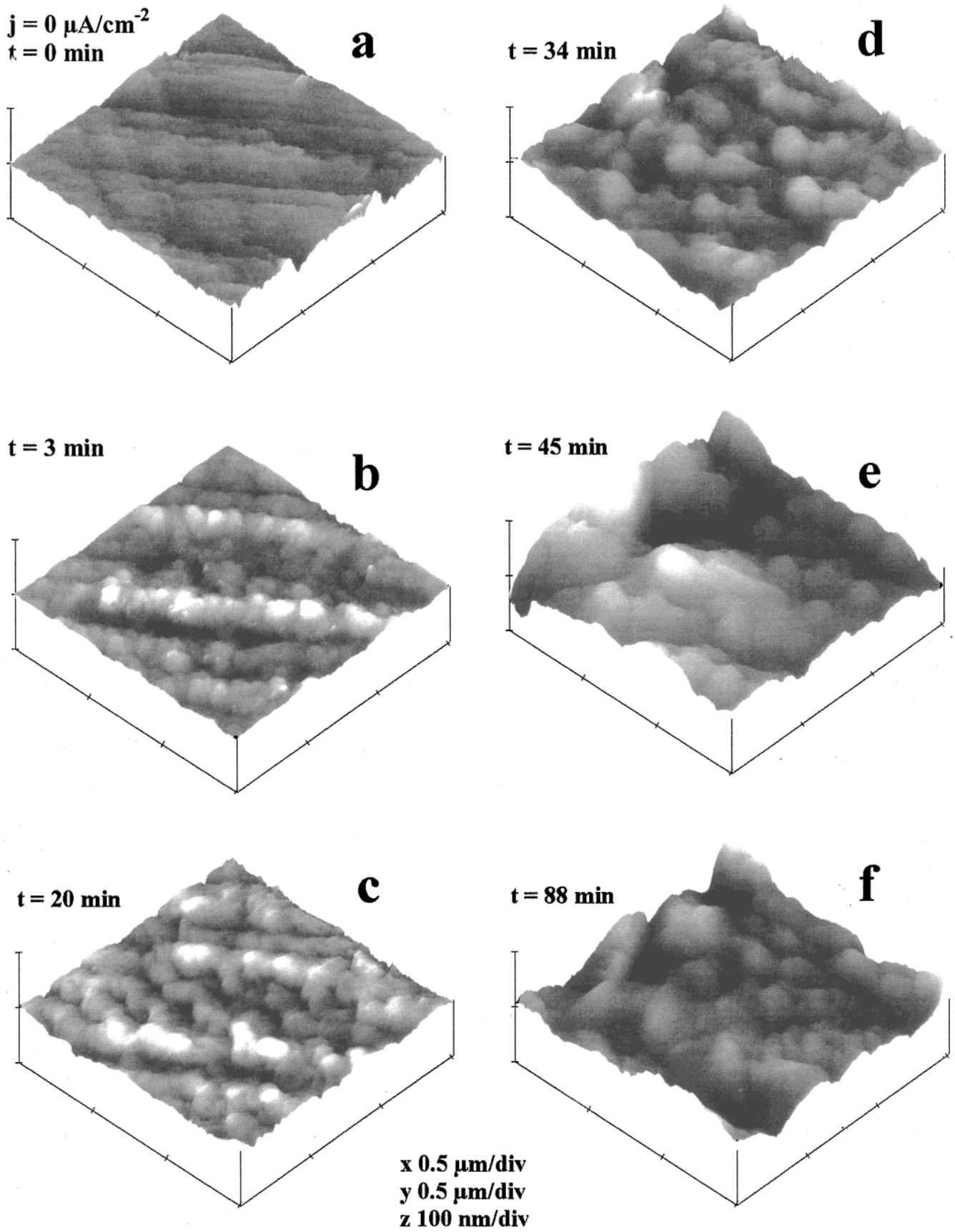

Figure 6. Sequential in situ STM images (1500 × 1500 nm^2, 3D view) of β-brass dealloying in aqueous 0.5 M sodium chloride at $j_L = 10$ μA/cm^2 and 298 K (b−f). Image a corresponds to the blank for $j = 0$ and $t = 0$, as indicated in the text. (a) -0.8 V $\leq E_{oc} \leq -0.5$ V; (b−f) $E = -0.360 \pm 0.003$ V.

yielding a low degree of surface coverage by hydrogen atoms. In contrast, the rate of zinc electrodissolution is considerably enhanced by the presence of chloride ions in the solution. In this case, ion pair bridging type zinc−chloride complexes

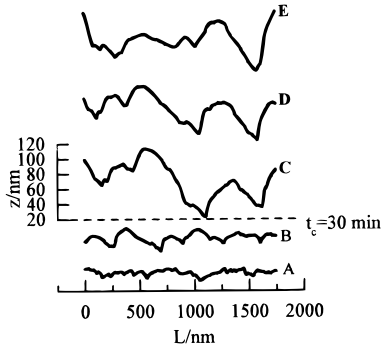

Figure 7. Representative cross section sequence (only five profiles are shown) for β-brass dealloying resulting from STM images depicted in Figure 6. The horizontal line indicates the separation between the two roughness regimes that are considered in the text.

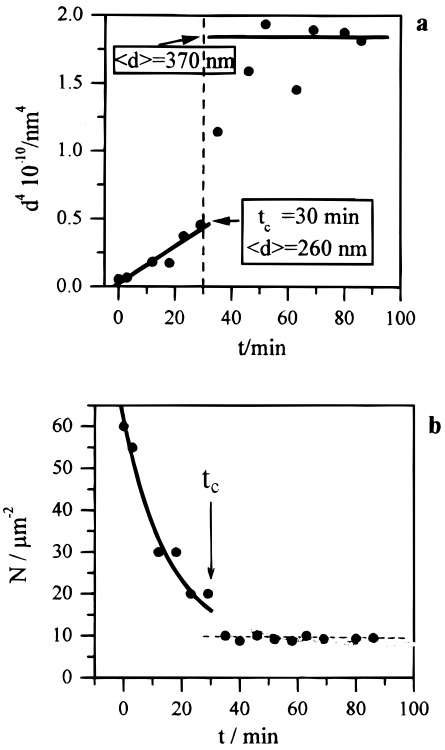

Figure 8. (a) Plot of d^4 vs t for copper island growth. (b) N vs t plot. The solid trace corresponds to the prediction of the $N \sim t^{-1/2}$ relationship that is valid for $t < t_c$.

catalyze the electron transfer.[18] The product of the overall anodic reaction is a chloride-containing zinc complex anion,

$$\beta\text{-brass(Zn,Cu)} + 4Cl^-(aq) = \beta\text{-brass(Cu)} + ZnCl_4^{2-}(aq) + 2e^- \quad (6)$$

The stability constant of $ZnCl_4^{2-}$(aq) ion is $K = 0.646$ at 298 K.[19]

On the other hand, the irreversible electroadsorption of chloride ions from aqueous sodium chloride on copper

$$Cu(s) + Cl^-(aq) = Cu(Cl)_{ad} + e^- \quad (7)$$

occurs close to -0.75 V, as has been determined in aqueous 0.3 M sodium chloride.[13] This value is more negative than $E_r = -0.120$ V[20] given for the reaction

$$2Cu(s) + 2Cl^-(aq) = Cu_2Cl_2 + 2e^- \quad (8)$$

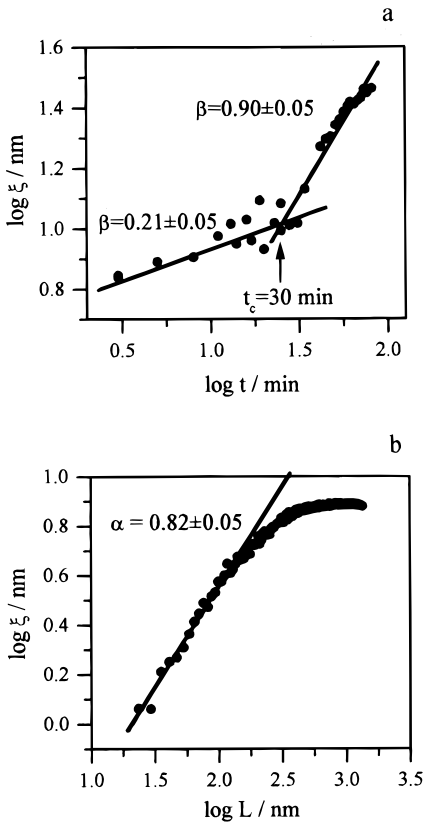

Figure 9. Data from the dynamic scaling analysis of sequential STM imaging cross sections: (a) log ξ vs log t plot, (b) log ξ vs log L plot.

From the standpoint of chloride ion adsorption on β-brass in aqueous sodium chloride, a distinction has to be made between chloride ion interaction with zinc and copper surface atom. In fact, considering the evolution of E_{oc} and the type of reaction products, it can be concluded that adsorption equilibrium conditions on copper remnants would be approached more easily than on electrodissolving zinc. Then, copper patches on the order of one monolayer thick should be covered by a diluted chloride ion lattice, as has been reported for copper[21] and copper remnants from dealloyed β-brass.[12] For these metallic surfaces a chloride ion lattice with a nearest neighbor distance close to 0.37 nm has been imaged by STM.

Accordingly, the spontaneous dealloying of β-brass in aqueous 0.5 M sodium chloride also leads to a copper-rich layer mostly covered by adsorbed chloride. As the size of this layer grows, the area of zinc available for reaction 4 is gradually diminished. Then, the instantaneous copper-to-zinc molar fraction ratio at the alloy surface is reflected by the value of E_{oc}. The copper-rich layer would act as an inhibitor, blocking surface sites for the slowest step of spontaneous dealloying that could be related to the rate of either reaction 5 or reaction 8 or to the rate of surface diffusion of copper−chloride species. This would explain the positive shift of the E_{oc} value, although this matter, which is beyond the scope of this work, deserves further consideration soon.

4.2. Applied Potential-Assisted β-Brass Dealloying. *4.2.1. Very Early Dealloying Stages ($t < t_1$).* Polarization curves (Figure 3) and potentiostatic current transient for β-brass dealloying (Figure 4) show that a charge equivalent to the electrodissolution of one monolayer of zinc atoms is involved before the anodic limiting current condition is attained. In fact, from the potentiostatic current transients recorded at $E = -0.45$ V (Figure 4) the electrodissolution of 0.5×10^{15} zinc atoms

requires a time $t_1 < 1$ s, leaving a number of surface copper atoms equivalent to 1 ML or thereabouts. Therefore, our constant current STM sequential imaging started from a β-brass surface largely covered by copper-rich patches that hinder zinc electrodissolution. In any case, as discussed in section 4.1., chloride ion adsorption should play a relevant role in β-brass dealloying in aqueous sodium chloride environments.

Initially, zinc electrodissolution can be expressed by the reaction

$$\beta\text{-brass(Zn,Cu)} + 4Cl^- \rightarrow \beta\text{-brass}(\square,x,y,z) + \beta\text{-brass(Cu,}x',y',z') + ZnCl_4^{2-}(aq) + 2e^- \quad (10a)$$

where a zinc atom is removed from the surface (site *x, y, z*) as a chloride-containing complex anion in solution leaving a vacancy (□) there, and a less coordinated copper atom remains at site *x′, y′, z′*. This copper atom can diffuse over a short distance on the surface to fill the neighbor vacancy at site *x, y, z*

$$\beta\text{-brass(Cu,}x',y',z') + \beta\text{-brass}(\square,x,y,z) \rightarrow \beta\text{-brass(Cu,Zn)} + \beta\text{-brass(Cu,}x,y,z) \quad (10b)$$

From this type of process a smooth surface richer in copper is attained. Reactions 10a and 10b may lead to an alloy surface fully covered by a copper-rich layer that would prevent further β-brass dealloying. Therefore, this simple explanation does not account for the steady β-brass dealloying under applied potential conditions.

4.2.2. Dealloying of β-Brass in the $t_1 < t < t_c$ and $t > t_c$ Ranges of Time. For $t_1 < t < t_c$ dealloying of β-brass in aqueous sodium chloride is characterized by the electrodissolution of zinc and simultaneous copper island growth as concluded from sequential STM images (Figure 7). At this stage, the analysis of electrochemical and STM imaging data indicate that the kinetics of dealloying is under surface diffusion control, and the evolution of solid−liquid interface attains a steady-state roughness regime (Figure 8).

On the other hand, the presence of chloride adsorbates enhances considerably the surface mobility of copper atoms,[22] favoring the growth of copper islands as β-brass dealloying proceeds. In this case, reaction 10b continues as follows:

$$\beta\text{-brass[Cu}(x,y,z)] + \beta\text{-brass[}n\text{Cu}(x'',y'',z'')] \rightarrow \beta\text{-brass[}(n+1)\text{Cu}(x'',y'',z'')] \quad (11)$$

Reaction 11 represents the surface diffusion of copper species to increase the size of a copper island. Accordingly, dealloying of β-brass is sustained by the enhancement of copper atom surface mobility, leaving reactive zinc atoms randomly distributed is space and time. Kinetic data indicate that reaction 11 is rate-determining. Therefore, β-brass dealloying (equation 10a), for $t_1 < t < t_c$ and $L < L_c$ produces a population of copper atoms sufficiently high to promote coalescence into three-dimensional (3D) copper islands (reaction 11). At this stage the development of a relatively smooth and stable interface and a coarsening of copper 3D islands are observed. Coarsening brings out zinc atoms from the underlying atom layers exposed to the solution so that zinc dealloying proceeds.

For $t > t_c$, however, a different situation arises as the surface diffusion of copper adatoms becomes insufficient to eliminate instabilities for $L > L_c$. This appears to be the case when a maximum lateral size by copper islands is attained. These islands in which lateral growth is largely hindered favor the appearance of β-brass patches where dealloying proceeds as a localized zinc electrodissolution process. In this case, dealloying results in void formation and copper islands both preferentially growing perpendicular to the alloy surface. Accordingly, deep voids, copper islands, and an equivalent amount of zinc complex anions in solution are produced, leading to an unstable roughness regime. This process can be formally represented by

$$\beta\text{-brass (m}\square) + \beta\text{-brass(}m\text{Cu)} + mZn(Cl_4)^{2-}(aq) + 4Cl^- \rightarrow \beta\text{-brass[}(m+1)\square] + \beta\text{-brass[}(m+1)\text{Cu}] + (m+1)Zn(Cl_4)^{2-}(aq) + 2e^- \quad (12)$$

followed by copper islands preferentially growing in height and coalescence of vacancies at the bottom of voids advancing in depth.

$$\beta\text{-brass[}\square(x,y,z)] + \beta\text{-brass[}n\square(x',y',z')] \rightarrow \beta\text{-brass[}(n+1)\square(x',y',z')] \quad (13)$$

For $L > L'$ growing voids are stabilized due to the high zinc atom surface concentration gradient established between bottom and top void sites, as has been demonstrated by X-ray photoelectron spectroscopy,[1] assisting further localized dealloying. Hence, reaction 13 implies a continuous advance of voids in depth into bulk alloy. From the stoichiometry of reactions 11−13 it can be concluded that the number of copper atoms forming islands is equal to the number of zinc atoms going into solution. Furthermore, considering that the atomic volumes of copper and zinc are almost the same,[16] the total volume of vacancies (voids) should also be equal to the total volume of copper islands. This equality is implicit in the cross section analysis of STM images considering the corresponding bearing planes (Figures 6 and 7).

4.2.3. The Experimental Activation Energy. The apparent activation energy for β-brass global dealloying derived from electrochemical data for $t_1 < t < t_c$ should be related to the rate-determining step (reaction 11). In fact, the fast zinc electrodissolution in aqueous sodium chloride is consistent with the molar solvation energy of Zn^{2+} ions ($\Delta G_s° = 137$ kJ/mol) that is very close to the molar cohesive energy of zinc ($\Delta G_c° = 131$ kJ/mol), and the molar free energy of formation of $[ZnCl]_4^{2-}$ complex ion (($\Delta G_f° = -469$ kJ/mol).[16,22,23]

On the other hand, the enthalpy change involved in reactions 10b and 11 depends on the number (n) of bond ruptures required for bond weakening of a copper atom for the alloy surface to promote copper atom surface diffusion. In general, this energy is estimated as $0.2\Delta H_s$, where ΔH_s is the molar enthalpy of sublimation. For copper, $\Delta H_s = 293$ kJ/mol, so that the expected activation energy would be 58.6 kJ/mol, a figure about 4 times greater than the experimental value $\Delta E_a^* = 12 \pm 4$ kJ/mol. To account for this difference, the contribution of copper−chloride ion interaction (reaction 8) should be taken into account in reactions 10b and 11. It is well-known that adsorbed chloride ions decrease the Cu−Cu bond energy, enhancing the rate of reactions 10b and 11.[24] In fact, the evaluation of ΔE_a^* from $\Delta H_s = 62.8$ kJ/mol for CuCl leads to $\Delta E_a^* = 12 \pm 4$ kJ/mol, a figure that agrees with our experimental value.

4.3. Interface Evolution and Coarsening. *4.3.1. Stable Roughness Regime.* For $t < t_c$ the scaling exponents resulted in $\alpha = 0.82 \pm 0.05$, $\beta = 0.21 \pm 0.05$, and $z = 3.7 \pm 0.4$. These figures are very close to $\alpha = 1$, $\beta = 0.25$, and $z = 4$ predicted for a process where curvature-driven surface diffusion is the main roughness relaxation determining the instantaneous interface width.[11] In this case, the interface evolution ($\partial h/\partial t$) is given

by the following stochastic equation[25]

$$\partial h/\partial t = -K\nabla^4 h + \eta + F \tag{14}$$

where K is a constant, η stands for the stochastic noise from the electrodissolution process that contributes to surface roughness, and F is the constant flux of Zn^{2+} ions going outward to the solution that is given by the limiting current density (Figure 3). Dealloying of β-brass can be described by eq 14 at coarse grained length scales, i.e., for scale lengths much greater than interatomic distances. For $t \gg t_1$, eq 14 predicts the $\langle d\rangle^4 \propto t$ dependence that was experimentally determined (Figure 7). The value of K obtained from the slope of the $\langle d^4\rangle$ vs t plot results in $K = 1.4 \times 10^{-23}$ cm^4/s.

The surface diffusion coefficient (D_m) of species involved in coarsening of copper islands can be estimated from the eq 14

$$D_m = Kk\mathrm{T}/2\gamma a^4 \tag{15}$$

From eq 15, using a curvature-independent surface tension $\gamma = 1000$ erg/cm^2, which is justified by the relatively large size of copper islands,[26,27] the lattice parameter of copper $a \cong 4 \times 10^{-8}$ cm, $T = 298$ K, and Boltzmann constant $k = 1.38 \times 10^{-16}$ erg/K, it results in $D_m \approx 10^{-10}$ cm^2/s. This figure is about 5 orders of magnitude greater than the value of the surface diffusion of copper atoms on pure copper in chloride ion-free aqueous solution.[28] This difference is consistent with the mobility enhancement of copper adatoms caused by the adsorption of chloride ions. In this case, the adsorbate would act as a contaminant layer promoting surface diffusion of copper atoms. For this enhancement of metal adatom surface diffusion several mechanisms have been advanced in the last years.[29]

The temperature dependence of the surface diffusion coefficient is given by the equation

$$D_m = D_{m,o} \exp(-\Delta E_a^*/RT) \tag{16}$$

As for $t > t_1$, dealloying of β-brass is characterized by a limiting anodic current density; let us assume that D_m is, in principle, independent of the applied potential in the dealloying potential range. Then, eq 16, taking $\Delta E_a^* = 12 \pm 4$ kJ/mol, results in $D_{m,o} \cong 10^{-8}$ cm^2/s. From the value of $D_{m,o}$ the average jump frequency ($1/\langle\tau\rangle$) can be estimated from the Einstein relationship

$$D_{m,o} = a^2/2\langle\tau\rangle \tag{17}$$

Thus, using $a^2 \cong 2 \times 10^{-15}$ cm^2 results in $1/\langle\tau\rangle \cong 10^7$ s, in agreement with a relaxation process several orders of magnitude slower than that expected from the Debye frequency, but much faster than that resulting for bare copper.[24]

The physical picture drawn by eq 14 implies that as vacancies in the alloy surface are produced they can be filled by the surface diffusion of copper atoms in order to decrease the surface free energy and increase the coordination number of copper atoms. Zinc atoms are rapidly removed from the alloy surface so that their contribution to vacancy filling should be negligible.

4.3.2. Unstable Roughness Regime. A different situation appears for $t > t_c = 30$ min as for $L > L_c$ surface diffusion relaxation becomes insufficient to stabilize the surface. In this case, voids increase in depth and the value of $\langle d\rangle$ resulting from the analysis of the STM topography remains nearly constant. Accordingly, the formation and growth of these voids change the roughness regime from stable to unstable, as concluded from the value $\beta = 0.90$ (Figure 8a). As discussed above, the rate of void growth is greater at void bottom because of the greatest concentration of zinc atoms near the alloy surface. In general, in those regions where the substrate is highly curved, surface tension can result in the development of irregularities.[27,30] Therefore, the interface exhibits a greater rate of "evaporation" at valleys than protrusions, so the relative height of the copper islands increases, i.e., "condensation" takes places at protrusions. In our case, the overall effect implies a negative surface tension coefficient in the Edwards−Wilkinson equation[31] turning the interface unstable.[11]

Hence, the complete interface evolution results from a competition between a surface diffusion contribution, which tends to stabilize the interface, and a negative surface tension contribution, which turns it unstable. Accordingly, eq 14 has to be modified as follows

$$\partial h/\partial t = -K\nabla^4 h + (-\nu)\nabla^2 h + \eta + F \tag{18}$$

where the first term on the right-hand side represents the surface relaxation by surface diffusion of copper adatoms, and the second term corresponds to void stabilization resulting from a negative surface tension. Therefore, eq 18 means that for the β-brass surface dissolving at constant F, there are two competing contributions in the rearrangement of the copper-rich β-brass surface. The term $-K\nabla^4 h$ tends to stabilize the interface by surface diffusion, whereas the term $(-\nu)\nabla^2 h$ turns the interface unstable, favoring void stabilization. These competing contributions that are represented by the linear terms in eq 18 originate a characteristic horizontal length, $L_c = (K/\nu)^{1/2}$. For $L < L_c$ (at the cluster surface scale), the term $-K\nabla^4 h$ dominates, and accordingly, the interface is stabilized by surface diffusion of copper adatoms. This process is enhanced by the formation of a CuCl adlayer. For $L > L_c$, the term $(-\nu)\nabla^2 h$ dominates, leading to void stabilization through the faster Zn electrodissolution at cavities. It should be noted that for the late stage of the process, images depicted in Figure 7 show slopes in the range 10−15° that might restrict the application of eq 18, which is strictly valid in the small slope approximation. However, it is known that linear terms are able to describe effectively the interface evolution of systems even in the case of strong instabilities.[32,33] The nonlinear terms dominate after a long crossover time.[33]

Considering the preceding arguments, the value of ν and the capillarity length Γ can be estimated. Thus, using $L_c = 3.7 \times 10^{-5}$ cm and $K = 1.4 \times 10^{-23}$ cm^4/s, the coefficient of the $\nabla^2 h$ term results in $\nu \approx 10^{-14}$ cm^2/s. On the other hand, the value of Γ can be estimated from

$$\Gamma = \nu/\omega \mathrm{k} \tag{19}$$

where ω is the atomic volume and k is the flux of Cu atoms on the surface. Considering $\omega \approx 10^{-23}$ cm^3/atom, and k $\approx 10^{13}$ atom/cm^2, eq 19 results in $\Gamma \approx 10^{-4}$ cm, a figure that is consistent with the values of $\langle d\rangle$ and L_c reported above. The value of k is estimated from $j_L = 10$ μA/cm,^{2} as the surface mobility of copper atoms is rate-controlling for β-brass dealloying.

In conclusion, the interface evolution of β-brass during dealloying at constant flux in the nanometer to micrometer range results from an interplay between surface diffusion and a negative surface tension that determines the crossover from the stable to the unstable regime. This explanation for the change in roughness regime for β-brass dealloying appears to be valid for other dealloying processes, such as those occurring for

copper−aluminum alloys[4] that result in nanoporous copper-rich remnants on the alloy that induce pitting.

Acknowledgment. This work was financially supported by PIP 4376 and PIP 0897/98 from Consejo Nacional de Investigaciones Científicas y Técnicas (CONICET), PICT 97-1993 and PICT 06-03251/98 from Agencia Nacional de Promoción Científica y Tecnológica (Argentina), and PI 1999/128 from Gobierno Autónomo Canario (Spain).

References and Notes

(1) Schreir, L.; Jarman, R. A.; Burnstein, G. T. *Corrosion*, Butterworth: Oxford, 1994; Vol. I.

(2) Oppenheim, I. C.; Trevor, D. J.; Chidsey, C. E. D.; Trevor, P. L.; Sieradzki, K. *Science* **1991**, *254*, 687.

(3) Sieradzki, K.; Corderman, R. R.; Shukla, K.; Newman, R. C. *Philos. Mag.* **1989**, *59*, 713.

(4) Dimitrov, N.; Mann, J. A.; Sieradzki, K. *J. Electrochem. Soc.* **1999**, *146*, 98.

(5) Newman, R. C.; Shahrabi, T.; Sieradzki, K. *Corros. Sci.* **1988**, *28*, 873.

(6) Burnstein, G. T.; Gao, G. *J. Electrochem. Soc.* **1994**, *141*, 912.

(7) Pickering, H. W.; Wagner, C. *J. Electrochem. Soc.* **1967**, *114*, 698.

(8) Fritz, J. D.; Pickering, H. W. *J. Electrochem. Soc.* **1991**, *138*, 3209.

(9) Sieradzki, K. *J. Electrochem. Soc.* **1993**, *140*, 2868.

(10) Family, F. *J. Phys. A* **1990**, *168*, 561.

(11) Barabási, A. L.; Stanley, H. E. *Fractal Concepts in Surface Growth*, Cambridge University Press: Cambridge, 1995.

(12) Morales, J.; Esparza, P.; González, S.; Vázquez, L.; Salvarezza, R. C.; Arvia, A. J. *Langmuir* **1996**, *12*, 500.

(13) *Metal Handbook, 9th Edition,* Vol. 4, Heat Treating of Copper Alloys; American Society for Metals, Metals Park, Ohio, 1981; p 719.

(14) Elsner, C. I.; Salvarezza, R. C.; Arvia, A. J. *Electrochim. Acta* **1988**, *33*, 1735.

(15) Glasstone, S.; Laidler, K. J.; Eyring, H. In *The Theory of Rate Processes*; McGraw-Hill: New York, 1941; Chapter 9, p 480.

(16) *Standard Potentials in Aqueous Solutions*; Bard, A. J., Parsons, R., Jordan, J., Eds; IUPAC, M. Dekker: New York, 1985.

(17) Brodd, R. J.; Leger, V. E. *Encyclopedia of Electrochemistry of the Elements*; Bard, A. J., Ed.; M. Dekker: New York, 1976; Vol. 5, Chapter 1.

(18) Blackledge, J.; Hush, N. S. *J. Electroanal. Chem.* **1963**, *5*, 435.

(19) Sillén, L. G.; Martell, A. E. *The Chemical Society Special Publication* No. 25, London, 1972.

(20) Bertocci, U.; Turner, D. R. *Encyclopedia of Electrochemistry of the Elements*; Bard, A. J., Ed.; M. Dekker: New York, 1974; Vol. 2, Chapter 6.

(21) Suggs, D.; Bard, A. J. *J. Am. Chem. Soc.* **1994**, *116*, 10725.

(22) *International Critical Tables*; Washburn, E. D., Ed.; McGraw-Hill: New York, 1930; Vol. 7, p 260.

(23) Parsons, R. *Handbook of Electrochemical Constants;* Butterworth: London, 1959; p 55.

(24) Bonzel, H. P. *Surface Physics of Materials*; Blakely, J. M., Ed.; Academic Press: New York, 1975; p 280.

(25) Wolf, D. E.; Villain, J. *Europhys. Lett.* **1990**, *13*, 389.

(26) Bikerman, J. J. *Physical Surfaces;* Academic Press: New York, 1970.

(27) Aveyard, R.; Haydon, D. A. *An Introduction to the Principles of Surface Chemistry,* Cambridge University Press: Cambridge, 1973.

(28) Aziz, S. G.; Vela, M. E.; Andreasen, G.; Salvarezza, R. C.; Hernández Creus, A.; Arvia, A. J. *Phys. Rev. B* **1997**, *56*, 4166.

(29) Galvele, J. R. In *Modern Aspects of Electrochemistry*; Conway, B. E., Bockris, J. O′M., White, R. E., Eds.; Plenum Press: New York, 1995; No. 27, p 233.

(30) Wiedner, D. E.; Schwartz, L. W.; Eley, R. R. *Colloid Interface Sci.* **1996**, *179*, 66, Eres, M. H.; Wiedner, D. E.; Schwartz, L. W. *Langmuir* **1999**, *15*, 5, 1859.

(31) Edwards, S. F.; Wilkinson, D. R. *Proc. R. Soc. London* **1982**, *A381*, 17.

(32) Cuerno, R., private communication.

(33) Cuerno, R.; Maksa, H. A.; Tomassone, S.; Harrington, S. T.; Stanley, H. E. *Phys. Rev. Lett.* **1995**, *75*, 4464.